Co-published by
Institute of Fluid-Flow Machinery
Polish Academy of Sciences
Committee on Thermodynamics and Combustion
Polish Academy of Sciences

http://www.imp.gda.pl/archives-of-thermodynamics/

Electro-osmotic and magnetohydrodynamic flow of Maxwell nanofluid over Darcy-Forchheimer porous medium with Soret-Dufour effects

Amudhini M, Poulomi De*

Department of Mathematics, School of Advanced Sciences, Vellore Institute of Technology, Chennai-600127, Tamilnadu, India
*Corresponding author email: poulomide12@yahoo.com

Received: 16.07.2024; revised: 09.09.2024; accepted: 08.10.2024

Abstract

In this study, we investigate the potential impacts of the thermo-diffusion and diffusion-thermo effects on electro-osmotic flow of Maxwell nanofluid across the stretching sheet. Magnetic and electric field over Darcy-Forchheimer flow and chemical reaction are also included. This study is vital in areas such as microfluidics, medical applications, and thermal management, where manipulating nanofluids under electromagnetic fields is essential. Through similarity transformation, the governing equations are turned into a collection of non-linear ordinary differential equations. The numerical results for the changed equations are obtained using the fifth order Runge-Kutta-Fehlberg technique with a shooting method. It has been established that if the Forchheimer number and electro-osmotic parameter increase, the velocity profile drops. As the diffusion-thermo effect grows so does the temperature profile. Similarly, the thermo-diffusion effect increases along with the concentration profile. The skin friction coefficient decreases by 10% and 23%, for the magnetic parameter increases from 0.4 to 2 and the Forchheimer number rises from 1 to 5, respectively. Additionally, with an increase in the Dufour number from 1.5 to 2, the Nusselt number decreases by 9%, while the Sherwood number increases by 33%. This research provides a more comprehensive analytical framework by integrating multiple physical effects such as Soret and Dufour effects, magnetic and electric fields, and porous media, thereby enhancing applications in microfluidic devices for precise fluid control, biomedical engineering for improved drug delivery and tissue engineering, thermal management for more efficient electronic cooling systems, environmental remediation for effective pollution control, and materials science for developing smart materials and nanocomposites.

Keywords: Maxwell nanofluid; Magnetohydrodynamics, Electro-osmotic forces; Darcy porous medium; Cross diffusion effects

Vol. 46(2025), No. 2, 69–81; doi: 10.24425/ather.2025.154907

Cite this manuscript as: M, A., & De, P. (2025). Electro-osmotic and magnetohydrodynamic flow of Maxwell nanofluid over Darcy-Forchheimer porous medium with Soret-Dufour effects. *Archives of Thermodynamics*, 46(2), 69–81.

1. Introduction

The capability to move a liquid caused by an electric field that is applied over a porous medium is referred to as electro-osmosis. The electro-osmotic force is induced from the collision of the electro-magnetic field that meets the ion in the liquid, which results in an overall movement of the fluid. Electro-osmotic flow is useful in a variety of domains, including microfluidics, chromatography, and electrokinetic separations. It is frequently used to regulate fluid motion in small-scale systems.

Nanofluids are made up of colloids containing nanoscale-sized particles, which are typically called nanoparticles that are dispersed throughout a base fluid like ethylene glycol, water or oil. Choi and Eastman [1] established the theoretical idea of

Nomenclature

a – parameter
B_0 – magnetic field strength, T
c_p – specific heat, J/(kg K)
c_s – concentration susceptibility, m^3/kg
C – concentration, mol/m^3
C_{fx} – coefficient of local skin friction
C_w – concentration at the surface of the sheet, mol/m^3
C_∞ – ambient concentration, mol/m^3
D_B – Brownian diffusion coefficient, m^2/s
D_T – thermophoresis diffusion coefficient, m^2/s
D_m – mass diffusivity, m^2/s
Df – Dufour number
e – electronic charge, C
E – electric field strength, N/C
E_1 – electric field parameter
Ec – Eckert number
E_x – applied electro-osmotic force, N
f – dimensionless stream function
F – non-uniform inertia force
Fr – Forchheimer number
k – thermal conductivity, W/(m K)
k_p – permeability of porous medium, m^2
k_1 – rate of chemical reaction
K – porosity parameter
K_B – Boltzmann constant, 1/(K mol)
K_T – thermo-diffusion ratio, 1/K
Kr – chemical reaction parameter
M – magnetic parameter
m_e – electroosmotic parameter
$\bar{n}_0$ – bulk concentration,
$\bar{n}^+$, $\bar{n}^-$ – cations and anions
Nb – Brownian motion parameter
Nt – thermophoresis parameter
Nu_x – local Nusselt number
Pr – Prandtl number
q_w, q_m – heat and mass flux, W/m^2, kg/(m^2 s)
Re_x – local Reynolds number
Sc – Schmidt number
Sr – Soret number
Sh_x – local Sherwood number
T – temperature of the fluid, K
T_w – temperature at the sheet's surface, K
T_∞ – ambient temperature, K
T_{av} – average temperature, K
u, v – fluid velocity in x- and y-direction, m/s
u_w – stretching velocity of sheet, m/s
U_{hs} – Helmholtz-Smoluchowski velocity, m/s
x, y – Cartesian coordinates, m
Z_v – charge balance
$(\cdot)'$ – differentiation with respect to η

Greek symbols

α – thermal diffusivity, m^2/s
β^* – Maxwell parameter
Γ – dimensional variable
$\bar{\Gamma}$ – electric potential, V
ε – dielectric permittivity
η – similarity variable
θ – temperature function
λ – fluid relaxation time, s
λ_e – Debye length, m
μ – dynamic viscosity of fluid, kg/(m s)
ν – kinematic viscosity of fluid, m^2/s
ξ – dimensionless similarity variable
ρ – density of fluid, kg/m^3
ρ_e – density of the total ionic energy, J/m^3
σ – electrical conductivity, S/m
τ – ratio of effective heat capacity of nanoparticle and base fluid
ϕ – concentration function

nanofluids by attempting to sustain different nanoparticles made from metals and metal oxides in various base fluids. Wong and De Leon [2] discussed existing and next-generation uses involving nanofluids, highlighting their better controlled heat transfer qualities and unique features. In a comparable manner, Jama et al. [3] evaluated the creation of metallic and nonmetallic nanofluids, in addition to the endurance of created nanofluids, plus also covered physical and thermal characteristics, as well as nanofluid applications. De et al. [4] evaluated the flow of nanofluid across the shrinking sheet utilizing thermal radiation and compared it to earlier studies. Kariko et al. [5] studied the flow of thixotropic nanofluid containing gyrotatic microorganisms along a vertical surface under convective conditions using active and passive controls. Yaseen et al. [6] analysed the flow of trihybrid nanofluid with gyrotactic microorganisms and Cattaneo-Christov model with a comparison of cone, wedge and plate, and concluded that heat transfer in a cone is greater than in other geometries. Akram et al. [7] investigated the flow of an Eyring-Powell hybrid nanofluid through an elliptical conduit with a concurrent entropy generation. Shah et al. [8] studied the magnetohydrodynamic (MHD) flow of Sutterby nanofluid via a Riga plate, including heat production. Shahzad et al. [9] investigated the peristaltic flow of hybrid nanofluid over an elliptical multi-stenotic artery, and the importance of the parameters was evaluated using a fuzzy environment. They also used entropy generation to reduce energy loss. Akbar et al. [10] explored the flow of Carreau-Yasuda nanofluid past an expanding sheet with the impacts of magnetic field, heat generation and variable thermal conductivity. Among these models, Maxwell fluid represents a type of non-Newtonian fluid. Maxwell fluids have a linear viscoelastic behaviour and are frequently employed for describing complicated fluids such as polymer melts or solutions that have both viscous and elastic effects. Knowing the rheological behaviour of Maxwell fluids is critical in a variety of industrial processes, including polymer and other material processing. Hayat et al. [11] explored the three-dimensional flow of Maxwell nanofluid together by employing convective and magnetic effects through a stretching sheet and numerically solved it using the homotopy analysis method. Through a porous expanding surface, Nagendramma et al. [12] reported the steady and incompressible transport of Maxwell nanofluid involving slip boundary conditions, thermal radiation and viscous dissipation. Using the Keller box method, Jamshed [13] numerically solved the problem of entropy generation in the MHD two-dimensional

flow of Maxwell nanofluid across an infinite horizontal surface containing viscous dissipation and thermal radiation effects. Murtaza et al. [14] used the Fourier sine transform and Laplace transform to precisely solve the problem of the electro-osmotic flow of Maxwell nanofluid along the existence of the field of electric charge into a conduit amid two plates which are parallel. Sultana et al. [15] examined the flow of a Maxwell hybrid fluid across a spinning disc in a porous media, taking into account suction effects and analyzing entropy generation.

The electromagnetohydrodynamic (EMHD) flow of fluid has been used in a variety of technological fields recently because of its benefits. The Lorentz force, which is produced by passing an electrical current over the channel in the direction of a perpendicular magnetic field, is the basis for the EMHD flow phenomenon. The electro-magnetohydrodynamic flow through the riga plate with buoyancy forces was studied by Pantokratoras and Magyari [16], who used a finite difference approach to tackle the issue. Buren and Jian [17] used the perturbation approach to solve the two-dimensional, unsteady, incompressible electro-magnetohydrodynamic flow in a microparallel channel containing slightly transverse corrugated walls. The simplified finite difference method (SFDM) was used by Irfan et al. [18] to solve the steady transport of nanofluid past the stretching sheet that is non-linear with electric and magnetic fields, porosity and heat generation/absorption. The electro-magnetohydrodynamic micropolar nanofluids involving slip conditions going along an expanded sheet are explored by Muhammad et al. [19] at its stagnation point flow.

Porous media, which are defined by interconnected void spaces, are used in a variety of engineering sectors, including environmental remediation, oil reservoir engineering, groundwater management and other areas. They aid in the comprehension and optimization of fluid flow in both naturally occurring and artificial systems. So, researchers are quite interested in it. An equation known as the Darcy law describes how fluid moves through a porous material. A fluid flow that defines the Darcy law is referred to as non-Darcy fluid movement. In spite of suction velocity and heat radiation, Raptis [20] studied the two dimensions and steady movement of the fluid with viscous properties through a medium that is porous on an infinite plate. Hayat et al. [21] use the homotopy analysis method (HAM) to solve the magnetohydrodynamic flow of a fluid that is not compressible but viscous through a porous medium via a vertically expanding sheet at its stagnation point. Qing et al. [22] investigated chemical reaction, heat radiation and magnetohydrodynamic flow of Casson nanofluid across a porous stretching/shrinking surface. Sajid et al. [23] studied the Maxwell nanofluid Darcy-Forchheimer transport across a linear stretching sheet combined with thermal conductivity, activation energy, as well as non-linear thermal radiation. Sangetha and De [24] studied the transport of a nanofluid containing microorganisms, implanted in a non-Darcy porous medium, as it passed over a convectively heated surface. Mohanty et al. [25−27] investigated the Darcy-Forchheimer flow of a hybrid nanofluid in a variety of scenarios, including flow past a moving needle under thermal radiation and Cattaneo-Christov heat flux, as well as past a disc influenced by Marangoni convection, thermo-solutal Marangoni convection, and activation energy, using entropy production analysis. Sohail et al. [28] investigated the flow of tri-hybrid pseudo-plastic fluid in the presence of a non-Darcy porous medium across a stretched sheet.

When distinct species or components within a mixture display varying rates of diffusion, this phenomenon is referred to as cross diffusion. Mass and thermal transfer processes, specifically in mixtures or multi-component fluids, are associated with the Soret and Dufour effects. The phenomenon wherein all the parts of a mixture travel with various speeds along a temperature gradient is referred to as the Soret effect, or thermal diffusion effect. The Dufour effect, sometimes referred to as diffusion-thermo effect, indicates that a temperature gradient can be induced by a concentration gradient and vice versa, resulting in the linked transfer of mass and heat. On a porous media with thermo-diffusion and diffusion-thermo effects, Moorthy and Senthilvadivu [29] investigated the thermal and mass transfer in a buoyancy-driven flow through a vertical surface. Using thermo-diffusion and diffusion-thermo effects, Partha et al. [30] explored the influence of double dispersion upon thermal and mass transfer by free convection over a vertical surface containing a non-Darcy conducting fluid filled with porous media. Ramzan et al. [31] researched on the mixed convective transport that occurs in a Maxwell nanofluid across a porous vertically expanded surface combining the thermo-diffusion and diffusion-thermo effects. Venkateswarlu and Narayana [32] researched the mixed convection flow of the Maxwell fluid through a vertical stretched sheet in combination with the context of magnetic field, Joule heating, chemical reactions and the Soret and Dufour effects. De [33] analysed the unsteady flow of a free convective Eyring-Powell magneto nanofluid mixed with Soret and Dufour effects past a semi-infinite vertical plate. Temjennaro and Hemanta [34] and Mathews and Hymavathi [35] considered an unsteady MHD flow with variable fluid properties.

1.1. Significance and uniqueness of the current work

This research peeps into the effects of the Soret and Dufour effects, magnetic and electric fields, and electro-osmotic force on the Darcy-Forcheimer flow and heat and mass transfer properties of Maxwell nanofluid. The novelty of this study is found in its detailed approach to modelling the intricate interactions among these factors, offering new insights into the behaviour of Maxwell nanofluids under the combined study of Soret-Dufour effect and electro-osmotic effect in the non-Darcy porous medium:

- A topic that has not been widely examined in past research.
- Understanding the concept of boundary layer can provide insights into overall effectiveness of nanofluids.
- It has potential applications in industry sectors such as cooling systems, crystal formation and magnetic drug targeting.
- It examines how non-Darcy porous media affect the heat and mass transfer in a Maxwell nanofluid, by filling a gap in literature and increasing our understanding of the complicated fluid behaviour of porous media.

- This offers the framework for future research to interact between the thermo-diffusion and diffusion-thermo effects in nanofluids, which helps to improve prediction accuracy in engineering.

The significance of the study lies in the following:

- Effective heat transmission may be achieved via thermo-magnetic pumping, which makes use of the combination of nanofluids with EMHD.
- Darcy-Forchheimer flow models are useful to investigate fluid flow over high velocity porous medium in water purification and desalination processes.
- Thermo-diffusion effect and diffusion-thermo effect in Maxwell fluid are used in cooling strategies in electronic devices.
- To optimize the transfer of heat in electro-kinetic heat exchangers, electro-osmotic force can be employed combined with Maxwell nanofluids.
- For physical comprehension, the velocity profile, temperature profile and concentration profile for various parameters are illustrated.

2. Mathematical formulation

Consider the steady, viscous, incompressible and Darcy-Forchheimer stream of Maxwell nanofluid over the porous medium. The flow is limited to the $y > 0$ plane. Nonetheless, the *x*-axis is tracked along the flow path, and the *y*-axis is selected orthogonal to the *x*-axis, in order to characterize the physical issue under consideration using the Cartesian coordinate system. Furthermore, an electroosmotic flow (EOF) is added to the sheet. The magnetic field occurs normally to the sheet, which is represented as $B = (0, B_0, 0)$, and the electric field $E = E(x)$ is generated from the applied magnetic field. Ohm's law $J = \sigma(E + V \times B)$ applies to both the magnetic and electric fields wherein V is the fluid velocity field, σ is the electrical conductivity and J is the Joule current. Moreover, the sheet is expanded over the path of the flow with a constant origin as a result of the action of opposing forces that are equal. Nevertheless, the fluid flow happened as a result of the sheet expanding in the line of *x*-axis (ref. Fig. 1, Zaher et al. [37]).

The governing equation of the Maxwell nanofluid flow equations are given below, with the aid of the boundary layer and above assumption which is obtained from Suraih Palaiah et al. [36]:

$$\frac{\partial u}{\partial x} + \frac{\partial v}{\partial y} = 0, \tag{1}$$

$$u\frac{\partial u}{\partial x} + v\frac{\partial u}{\partial y} = \nu\frac{\partial^2 u}{\partial y^2} - \lambda\left(u^2\frac{\partial^2 u}{\partial x^2} + v^2\frac{\partial^2 u}{\partial y^2} + 2uv\frac{\partial^2 u}{\partial x \partial y}\right) - \frac{\sigma}{\rho c_p}\left({B_0}^2 u - EB_0\right) - \frac{\mu}{k_p}u - \frac{F}{\sqrt{k_p}}u^2 + \rho_e E_x, \tag{2}$$

$$u\frac{\partial T}{\partial x} + v\frac{\partial T}{\partial y} = \frac{k}{\rho c_p}\frac{\partial^2 T}{\partial y^2} + \frac{\mu}{\rho c_p}\left(\frac{\partial u}{\partial y}\right)^2 + \tau\left[D_B\frac{\partial C}{\partial y}\frac{\partial T}{\partial y} + \frac{D_T}{T_\infty}\left(\frac{\partial T}{\partial y}\right)^2\right] + \frac{\sigma}{\rho c_p}(uB_0 - E)^2 + \frac{D_m K_T}{T_m}\frac{\partial^2 T}{\partial y^2}, \tag{3}$$

$$u\frac{\partial C}{\partial x} + v\frac{\partial C}{\partial y} = D_B\frac{\partial^2 C}{\partial y^2} + \frac{D_T}{T_\infty}\frac{\partial^2 T}{\partial y^2} + \frac{D_m K_T}{T_m}\frac{\partial^2 T}{\partial y^2} - k_1(C - C_\infty). \tag{4}$$

In the above Eqs. (1)–(4), μ, ν, λ, ρ, k_p, σ, c_p, D_B, D_T, k_1 represent the viscosity, kinematic viscosity, relaxation time, density, permeability of the porous medium, electrical conducivity, specific heat, Brownian motion coefficient, thermophoresis diffusion coefficient and chemical reaction rate.

The continuity principle is embodied in Eq. (1), which guarantees mass conservation. The momentum equation is given by Eq. (2), where the second term on the right-hand side represents

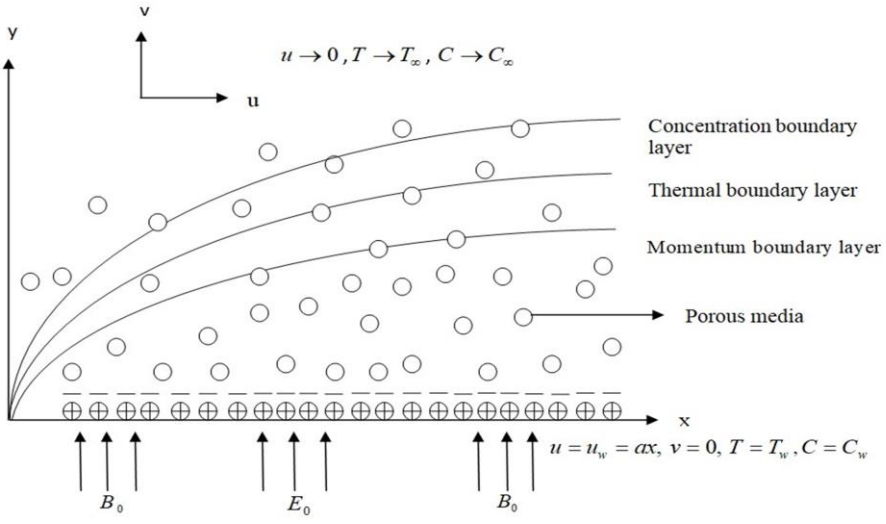

Fig. 1. Illustration of fluid flow.

the Maxwell fluid, the third term describes the behaviour of the magnetic and electric fields, the fourth term is due to the impact of porous media, the next term characterizes the Darcy-Forchheimer flow, and the last term refers to the electro-osmotic force. The energy equation is given by Eq. (3), where the second term on the right denotes the viscous dissipation, the third term represents the essence of Brownian motion and thermophoresis effect, the next term refers to the Joule heating and the last term denotes the Dufour effect. A chemical process is represented by the term at the right of Eq. (4); before that, the Soret effect is denoted, which appears in the concentration equation.

For the above Eqs. (1)–(4), the boundary conditions are (Suraih Palaiah et al. [36]):

$$u = u_w = ax, \quad v = 0, \quad T = T_w, \quad C = C_w \quad \text{at} \quad y = 0,$$
$$u \to 0, \quad T \to T_\infty, \quad C \to C_\infty \quad \text{as} \quad y \to \infty. \tag{5}$$

The boundary conditions in Eq. (5) are governed by the surface temperature and concentration, with consistent velocity at the surface and by the ambient temperature and concentration with zero velocity at the outer edge of the boundary layer.

The partial differential equations (PDEs) (2)–(4) are converted into the ordinary differential equations (ODEs) by the following similarity transformations from Suraih Palaiah et al. [36]:

$$\eta = \sqrt{\frac{a}{v}}y, \quad u = axf'(\eta), \quad v = -\sqrt{av}f(\eta),$$
$$\theta(\eta) = \frac{T-T_\infty}{T_w-T_\infty}, \quad \phi(\iota) = \frac{C-C_\infty}{C_w-C_\infty}. \tag{6}$$

3. Examining electro-osmotic flow using boundary layer flow

The following can be obtained from the Gaussian law (Zaher et al. [37]):

$$\nabla \cdot E = \frac{\rho_e}{\varepsilon}, \tag{7}$$

where ε is the dielectric permittivity and ρ_e is the overall ionic energy density. Since it is believed that the electric field is conservative, the electric potential $\bar{\Gamma}$ is written as follows:

$$E = -\nabla\bar{\Gamma}. \tag{8}$$

Substituting Eq. (8) into Eq. (7)

$$\nabla \cdot \nabla\bar{\Gamma} = \nabla^2\bar{\Gamma} = -\frac{\rho_e}{\varepsilon}. \tag{9}$$

The Boltzmann distribution is described by the total density of charged particles, which is symbolized as (Abdelsalam et al. [38]):

$$\rho_e = -Z_v e(\bar{n}^- - \bar{n}^+), \tag{10}$$

where the term $\bar{n}^- = \bar{n}_0 e^{-\frac{eZ_v}{T_{av}K_B}\bar{\Gamma}}$ denotes the anions and $\bar{n}^+ = \bar{n}_0 e^{\frac{eZ_v}{T_{av}K_B}\bar{\Gamma}}$ denotes the cations. The Debye-Huckel linearization principle states that $\frac{eZ_v}{T_{av}K_B} << 1$. Reducing Eq. (10), we get

$$\rho_e = \frac{\varepsilon}{\lambda_e^{\,2}}\bar{\Gamma}, \tag{11}$$

where $\partial/\partial x \to 0$ in Eq. (9), leading to:

$$\frac{d^2\bar{\Gamma}}{dy^2} = \frac{1}{\lambda_e^2}\bar{\Gamma}. \tag{12}$$

Using the following transformation

$$\Gamma = \frac{\bar{\Gamma}}{\xi}, \quad \eta = \sqrt{\frac{a}{y}}y,$$

Eq. (12) is transformed to:

$$\frac{d^2\Gamma}{d\eta^2} = m_e^2\Gamma,$$

where $m_e = \sqrt{\frac{v}{a}}\frac{1}{\lambda_e}$ is the electro-osmotic parameter.

The outcome of the above equation with boundary conditions $\Gamma = 1$ at $\eta = 0$ and $\Gamma \to \infty$ at $\eta \to \infty$ is

$$\Gamma = \exp(-m_e\eta). \tag{13}$$

The transformed ordinary differential Eqs. (2)–(4) are:

$$f''' - \beta^*(f^2f''' - 2ff'f'') + ff'' - f'^2 + M(E_1 - f') - Kf' - \mathrm{Fr}f'^2 + U_{hs}m_e^2\mathrm{e}^{-m_e\eta} = 0, \tag{14}$$

$$u\theta'' + \mathrm{Pr}\,f\,\theta' + \mathrm{Pr}\,\mathrm{E}\,\mathrm{c}f''^2 + \mathrm{Pr}\,N\,b\theta'\phi' + \mathrm{Pr}\,N\,t\theta'^2 + \mathrm{Pr}\,M\,\mathrm{Ec}(f' - E_1)^2 + \mathrm{Pr}\,\mathrm{D}\,\mathrm{f}\phi'' = 0,. \tag{15}$$

$$\phi'' + \mathrm{Sc}f\phi' + \frac{Nt}{Nb}\mathrm{Sc}\theta'' + \mathrm{SrSc}\theta'' - \mathrm{KrSc}\phi = 0. \tag{16}$$

The boundary conditions for the above equations are:

$$f(0) = 0, f'(0) = 1, \ \theta(0) = 1, \ \varphi(0) = 1 \text{ at } \eta = 0,$$
$$f'(\infty) \to 0, \ \theta(\infty) \to 0, \ \varphi(\infty) \to 0 \text{ as } \eta \to \infty. \tag{17}$$

The dimensionless parameters in Eqs. (14)–(16) are given below: $\beta^* = \lambda a$ is a Maxwell fluid parameter, $M = \frac{\sigma B_0}{\rho a}$ is a magnetic parameter, $E_1 = \frac{E}{B_0 u_w}$ is the electric field parameter, $K = \frac{\mu}{k_p a}$ is the porosity parameter, $\mathrm{Fr} = \frac{Fx}{\sqrt{k_p}}$ is the Forchheimer number, $U_{hs} = \frac{\varepsilon\xi E_x}{\nu u_w}$ is the Helmholtz-Smoluchowski velocity, $m_e = \sqrt{\frac{a}{v}}\frac{1}{\lambda_e}$ is the electro-osmotic parameter, $\mathrm{Pr} = \frac{\nu}{\alpha}$ is the Prandthl number, $\mathrm{Ec} = \frac{u_w^2}{c_p(T_w - T_\infty)}$ is the Eckert number,

$Nb = \frac{\tau D_B}{\nu}(C_w - C_\infty)$ is the Brownian motion parameter, $Nt = \frac{\tau D_T}{\nu T_\infty}(T_w - T_\infty)$ is the thermophoresis parameter, $\mathrm{Df} = \frac{D_m K_T}{\nu c_s c_p}\frac{(C_w - C_\infty)}{(T_w - T_\infty)}$ is the Dufour number, $\mathrm{Sc} = \frac{\nu}{D_B}$ is the Schmidt number, $\mathrm{Sr} = \frac{D_m K_T}{\nu T_m}\frac{(T_w - T_\infty)}{(C_w - C_\infty)}$ is the Soret number, $\mathrm{Kr} = \frac{k_1}{a}$ is the chemical reaction parameter.

The local skin-friction coefficient (C_{fx}), the Nusselt number (Nu_x) and the Sherwood number (Sh_x) for the current study are as follows:

$$C_{fx} = \frac{\tau_w}{\rho u_w^2}, \quad \mathrm{Nu}_x = \frac{x q_w}{k(T_w - T_\infty)}, \quad \mathrm{Sh}_x = \frac{x q_m}{D_B(C_w - C_\infty)}, \tag{18}$$

where $\tau_w = \mu\left(\frac{\partial u}{\partial y}\right)_{y=0}$ is the wall shear stress, $q_w = -k\left(\frac{\partial T}{\partial y}\right)_{y=0}$ is the heat flux and $q_m = -D_B\left(\frac{\partial C}{\partial y}\right)_{y=0}$ is the mass flux.

Equations (18) are reduced to non-dimensional form as follows:

$$C_{fx}\mathrm{Re}_x^{\frac{1}{2}} = f''(0), \quad \mathrm{Nu}_x\,\mathrm{Re}_x^{-\frac{1}{2}} = -\theta'(0),$$
$$\mathrm{Sh}_x\,\mathrm{Re}_x^{-\frac{1}{2}} = -\varphi'(0), \tag{19}$$

where $\mathrm{Re}_x = ax^2/\nu$.

4. Numerical methods

Employing the fifth order Runge-Kutta-Fehlberg method combined with a shooting method, one can determine the accepted finite values of $\eta \to \infty$ and solve the non-linear ODEs (14)–(16). The values n_∞ are found by picking a set of initial estimate values for various physical variables and repeating the method unless two consecutive values of $f''(0)$, $\theta'(0)$ and $\varphi'(0)$ are deviated by less than a specified tolerance. This approach reduces Eqs. (14)–(16) to seven simultaneous ODE's with the following consequences:

$$f_1' = f_2,$$
$$f_2' = f_3,$$
$$f_3' = \frac{1}{1-\beta^* f_1^2}\left[f_2^2 - 2\beta^* f_1 f_2 f_3 - f_1 f_3 - M(E_1 - f_2) - K f_2 - \mathrm{Fr} f'^2 + U_{hs} m_e^2 \mathrm{e}^{-m_e^2 \eta}\right],$$
$$f_4' = f_5,$$
$$f_5' = -\left(\frac{\mathrm{Pr}}{l} - \mathrm{PrDfSc}\frac{Nt}{Nb} - \mathrm{PrDfScSr}\right)[f_1 f_5 + \mathrm{Ec} f_3^2 + Nb f_5 f_7 + Nt f_5^2 + M\mathrm{Ec}(f_2 - E_1)^2 - \mathrm{DfSc} f_1 f_7 + \mathrm{Df} Kr\, f_6],$$
$$f_6' = f_7,$$
$$f_7' = -\mathrm{Sc} f_1 f_7 - \frac{Nt}{Nb} f_5' - \mathrm{SrSc} f_5' + Kr\mathrm{Sc} f_6.$$

Here $f_1 = f$, $f_2 = f'$, $f_3 = f''$, $f_4 = \theta$, $f_5 = \theta'$, $f_6 = \varphi$, $f_7 = \varphi'$.

The following are the transformed boundary conditions:

$$f_1 = 0, \quad f_2 = 1, \quad f_3 = c_1, \quad f_4 = 1$$
$$f_5 = c_2, \quad f_6 = 1, \quad f_7 = c_3 \quad \text{at} \quad \eta = 0,$$
$$f_2 = 0, \quad f_4 = 0, \quad f_6 = 0 \quad \text{at} \quad \eta \to \infty.$$

The values $f''(0)$, $\theta'(0)$ and $\varphi'(0)$ are found using the initial guess values c_1, c_2, and c_3 until they satisfy the boundary conditions. The fifth order Runge-Kutta method is employed to achieve highly accurate results with a convergence threshold of 10^{-8}. This ensures that the numerical solutions are precise and reliable, allowing for a detailed understanding of the fluid flow behaviour.

5. Results and discussion

The graphs represented in this section depict the significance of the parameters mentioned in Eqs. (14)–(16) with the help of boundary condition in Eq. (17) for the steady flow conduct, temperature and concentration distribution. The Nusselt numbers for a subset of Prandtl numbers are compared in order to validate the current study. It is assumed that $Nt = Nb = 0.1$, $\mathrm{Sc} = 1.0$ and all other parameters are set to zero. There is an excellent compromise in contrast to the previously published research of [26–28] and it is presented in Table 1.

Table 1. Comparative analysis of outcomes for the Nusselt number − θ'(0) with *Nt* = *Nb* = 0.1, Sc = 1.0; all other parameters set to zero.

Pr	Wang [39]	Reddy Gorla et al. [40]	Khan and Pop [41]	Present
0.07	0.0656	0.0656	0.0663	0.06592
0.2	0.1691	0.1691	0.1691	0.16889
0.7	0.4539	0.5349	0.4539	0.45465
2.0	0.9114	0.9114	0.9113	0.91132

Furthermore, it is shown that when Pr values rise, heat transfer improves. The study's findings are illustrated graphically for particular parameter ranges such as: $0.5 \le \beta^* \le 12.5$, $0.5 \le M \le 8.5$, $0.1 \le E_1 \le 0.4$, $1 \le K \le 5$, $0.3 \le \mathrm{Fr} \le 5$, $0.5 \le U_{hs} \le 5.0$, $0.4 \le m_e \le 9.0$, $5.0 \le \mathrm{Pr} \le 9.0$, $0 \le \mathrm{Ec} \le 0.3$, $0.3 \le Nb \le 11.0$, $0.8 \le Nt \le 3$, $0.1 \le \mathrm{Df} \le 2.5$, $2 \le \mathrm{Sc} \le 4$, $0.05 \le \mathrm{Sr} \le 0.5$, and $0.3 \le Kr \le 4.5$. These intervals were chosen to guarantee manageable computation and ensure convergence under the specified conditions.

The influence of Maxwell fluid parameter (β^*) on the velocity profile is shown in Fig 2. The relaxation time (λ) increases with an increase in β^*, which enhances the fluid's elastic nature. As a result, the viscosity rises, causing greater resistance to flow and the velocity profile falls. Physically, this represents the greater dominance of elastic effects, which slow down the fluid velocity since it takes longer to recover after deformation. The same trend occurs in Suraih Palaiah et al. [36].

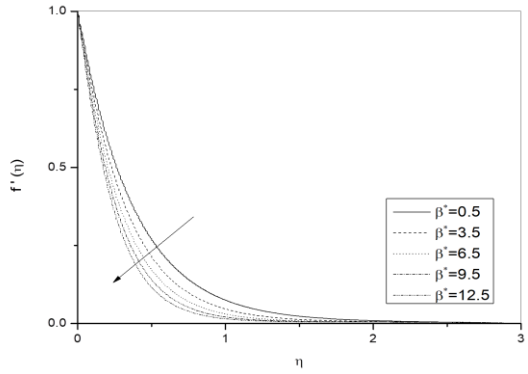

Fig. 2. Effect of Maxwell fluid parameter on velocity profile.

Figure 3 illustrates the impact of magnetic parameter (M) upon velocity distribution. The force that acts on the fluids is the Lorentz force which opposes the fluid velocity. This causes an increase in the resistance of flow and a fall in the velocity profile. A similar pattern is observed in the study of Jamshed [13].

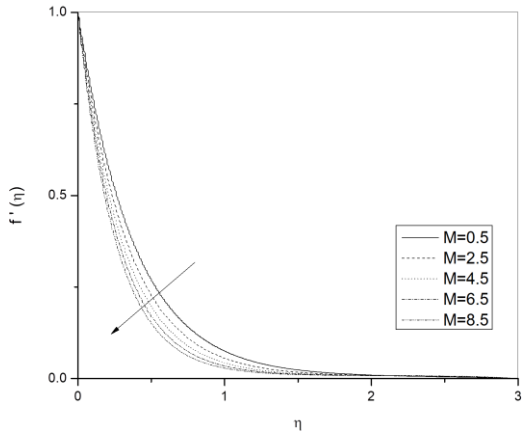

Fig. 3. Contribution of magnetic parameter to velocity distribution.

The influence of the porosity parameter (K) on the velocity profile is displayed in Fig. 4. The flow resistance rises as the porosity parameter grows because the voids in the porous medium get bigger. As an outcome, the velocity profile gets decreased. A comparable pattern is noted by Mohanty et al. [27]. Figure 5 shows the impact of the Forchheimer number (Fr) on the velocity distribution. It is discovered in which the Forchheimer number rises, the boundary layer thickens because the Forchheimer number represents inertial drag effects in porous media. This results in adding resistance to the fluid motion. As a result, the velocity profile decreases. The same trend is observed in the work of Mohanty et al. [27].

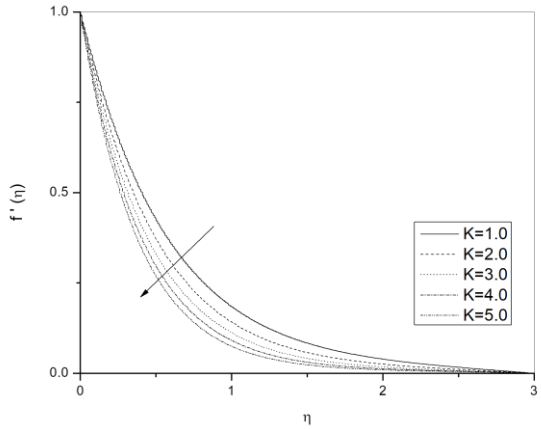

Fig. 4. Effect of porosity parameter on velocity distribution.

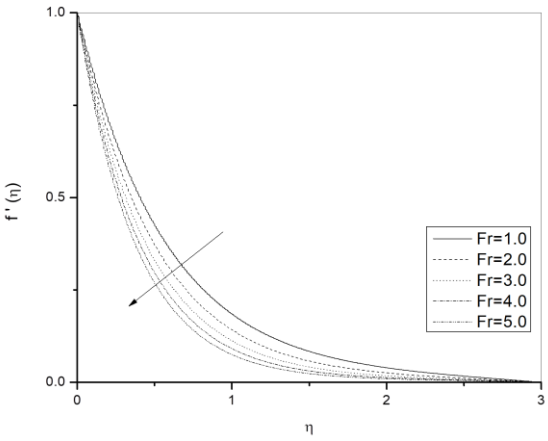

Fig. 5. Effect of Forchheimer number on velocity distribution.

Figure 6 illustrates how the velocity profile is affected by the Helmholtz-Smoluchowski velocity (U_{hs}). As the Helmholtz-Smoluchowski velocity rises, it causes particles that are charged in electric fields produced in the electro-osmotic flow to travel at an average faster velocity. That results in increases of the velocity distribution by reducing the resistance. The similar pattern is noted by Zaher et al. [37].

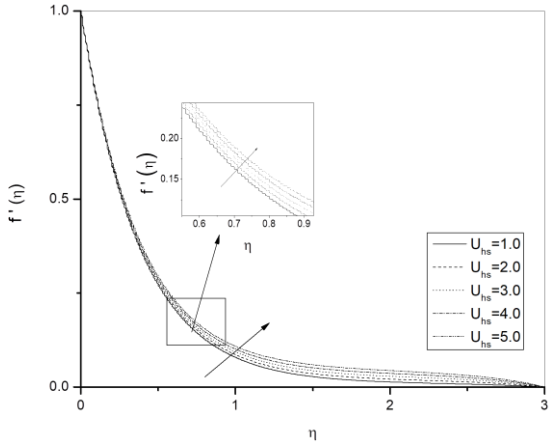

Fig. 6. Effect of Helmholtz-Smoluchowski velocity on velocity profile.

Figure 7 depicts the consequence of electro-osmotic parameter (m_e) upon the velocity profile. As the electro-osmotic parameter increases it leads to creating an electric double layer (EDL) in the flow which strengthens the electrostatic forces near the charged surface by creating more drag. This increases resistance of the fluid flow, and thereby decreases the velocity distribution. A comparable trend is noted in the study conducted by Hegazy et al. [42].

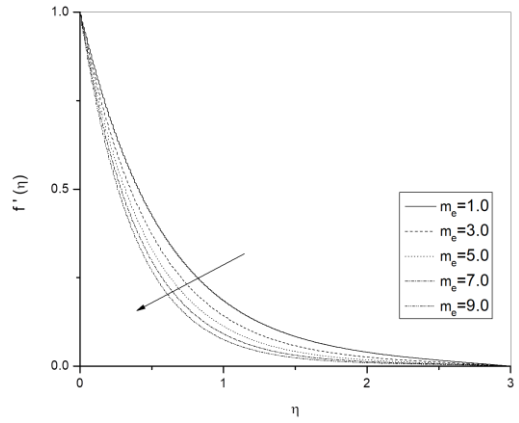

Fig. 7. Effect of electro-osmotic parameter on velocity distribution.

As seen in Fig. 8, a rise in the temperature distribution is implied by a booster in the Prandtl number. Thermal diffusivity becomes more prevalent over kinematic viscosity as by definition, as the Prandtl number increases. The same pattern is observed by Kumar et al. [43].

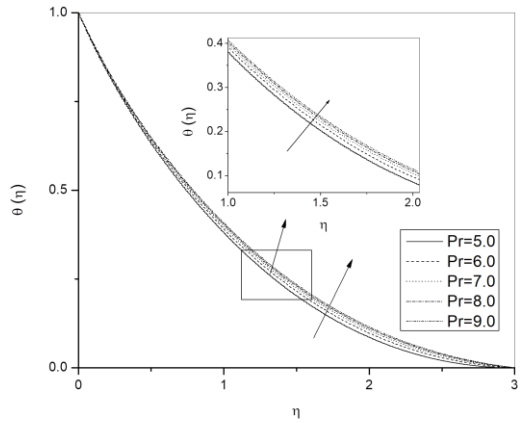

Fig. 8. Effect of Prandtl number on temperature profile.

A growth in the Eckert number (Ec) indicates a decrease in the temperature profile, as shown in Fig. 9. The kinetic energy dissipation may be of greater importance in the flow than the heat transmission if the Eckert number rises. This could contribute to a drop in the temperature distribution by decreasing the capacity of kinetic energy conversion to thermal energy. This trend is occurred in Palanimani [44]. Figure 10 demonstrates the way that the thermophoresis parameter (Nt) consequences the temperature profile. The temperature distribution rises when Nt is increased because it is found that nanoparticles at the hot boundary layer are being moved in the direction of the cold fluid by the thermophoretic force. This force redistributes the heat and results in an increase of the temperature profile. A comparable pattern is noted in Ragupathi et al. [45]. Figure 11 depicts the effects of the Dufour number (Df) on temperature profile. Thermal diffusivity to mass diffusivity is expressed as a Dufour number. An increased Dufour number suggests that thermal diffusivity is more vital than mass diffusivity. It follows that a rise in the temperature profile is the outcome of heat transfer effects predominating over mass transfer effects. The same trend occurs in De [33].

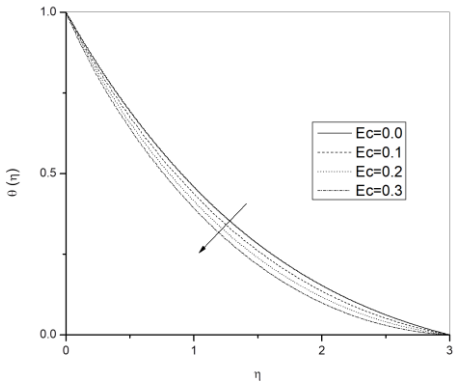

Fig. 9. Effect of Eckert number on temperature profile.

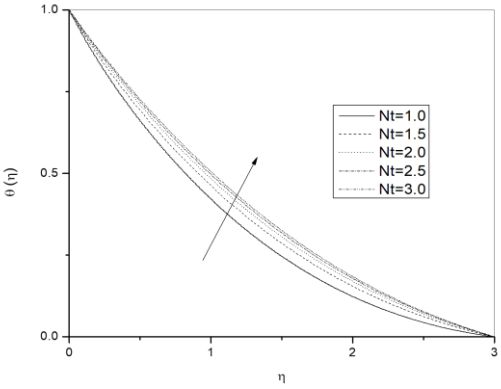

Fig. 10. Effect of thermophoresis parameter on temperature profile.

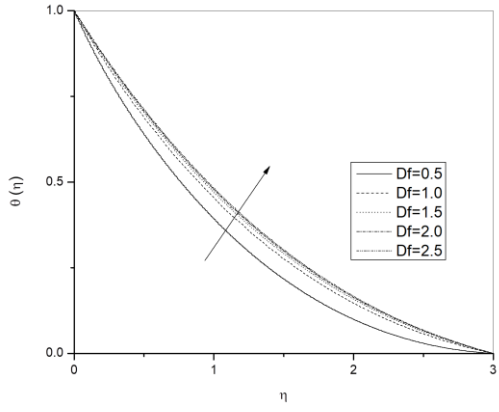

Fig. 11. Effect of Dufour number on temperature profile.

Figure 12 shows how a change in the Brownian motion parameter (Nb) causes the concentration distribution to increase. The chaotic movement of nanoparticles in suspension in the carrier fluid is called Brownian motion. A rise in Brownian motion results in moving particles more vigorously and randomly and hence, evens out the concentration of particles across the fluid by reducing the difference between high and low concentration regions. Thus, as the value of Nb increases, the concentration decreases. A similar pattern is observed by Awan et al. [46].

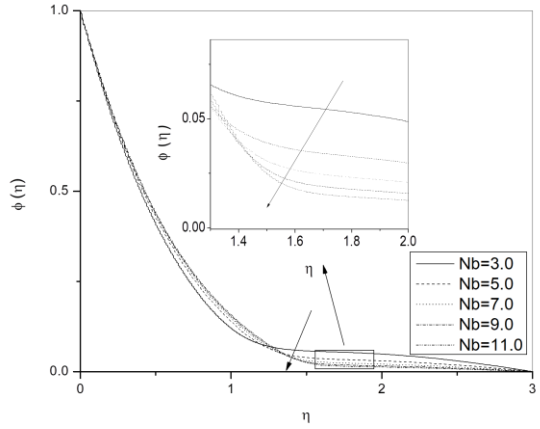

Fig. 12. Effect of Brownian motion parameter on concentration profile.

The consequence of Schmidt number (Sc) on concentration distribution is revealed in Fig. 13. The kinematic viscosity to mass diffusivity ratio is represented as the Schmidt number. A rise in Schmidt number raises kinematic viscosity and lowers mass diffusivity and it results in a fall in concentration gradients and a decrease in concentration profiles.

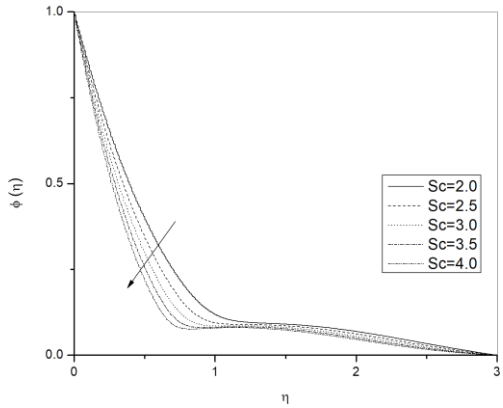

Fig. 13.The influence of Schmidt number on concentration distribution.

Soret number's influence over the concentration profile is shown in Fig. 14. A boost in the Soret number (Sr) leads to an enhancement in the concentration profile because thermal diffusion has a major impact on the flow of species within a fluid mixture, leading the concentration profile to rise. A similar pattern is observed by De [33]. Figure 15 shows the impact of chemical reaction parameter (Kr) on the concentration distribution. An increase in chemical reaction parameter causes the concentration profile to decrease because the reactant concentrations may fall more rapidly, resulting in a more noticeable reduction in concentration gradients within the fluid. The same trend is found by Raza et al. [47].

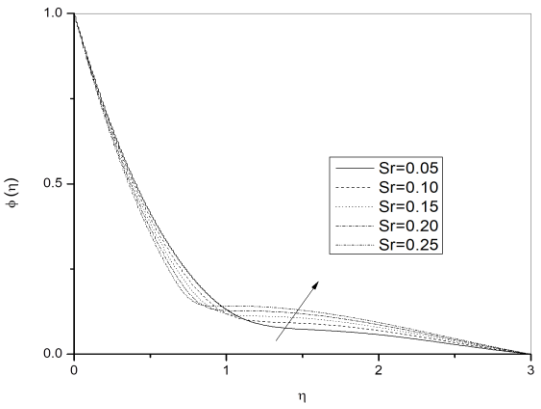

Fig. 14.Effect of Soret number on concentration profile.

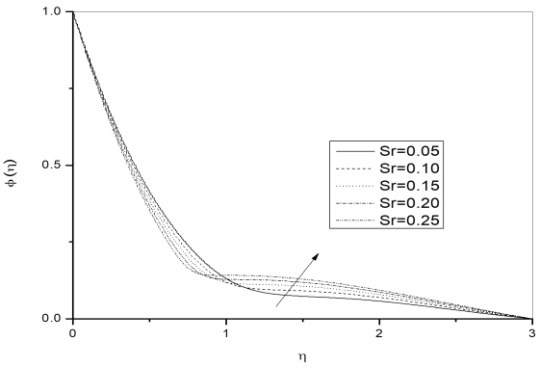

Fig. 15. Effect of Soret number on concentration profile.

Table 2 describes the skin friction coefficient for different parameters including the Maxwell fluid parameter, magnetic field parameter, electric field parameter, porosity parameter, Forchheimer number, Helmholtz-Smoluchowski velocity and electro-osmotic parameter. An increase in Maxwell fluid parameter, magnetic parameter, porosity parameter, Forchheimer number and electro-osmotic parameter decreases the skin friction coefficient due to the reduction in velocity gradient near the wall, whereas an increase in electric field parameter and Helmholtz-Smoluchowski velocity increases the skin friction coefficient. Table 3 represents the Nusselt number and Sherwood number for different parameters including the Prandtl number, Eckert number, Brownian motion parameter, thermophoresis parameter, Dufour number, Schmidt number, Soret number and chemical reaction parameter. Increasing the Prandtl number, thermophoresis parameter, Dufour number and Soret number reduces the Nusselt number by decreasing the convective heat transfer and increases the Sherwood number by strengthening mass transfer. Conversely, an increase in Eckert number, Brownian motion, Schmidt number and chemical reaction parameter leads to an increase in Nusselt number and a decrease in Sherwood number.

Table 2. Skin friction coefficient for different parameters.

β^*	M	E_1	K	Fr	U_{hs}	m_e	$f''(0)$
0.5	0.5	0.2	3.0	0.3	0.5	0.4	-2.15952
1.5							-2.27339
2.5							-2.38406
0.5	0.4						-2.14594
	1.2						-2.25369
	2.0						-2.35878
	0.5	0.1					-2.18365
		0.3					-2.13543
		0.5					-2.08362
		0.2	1.0				-1.63064
			3.0				-2.15952
			5.0				-2..58216
			3.0	1.0			-2.26370
				3.0			-2.53863
				5.0			-2.78723
				0.3	1.0		-2.14220
					3.0		-2.07310
					5.0		-2.00428
					0.5	1.0	-2.14424
						3.0	-2.17148
						5.0	-2.17659

Table 3. Nusselt and Sherwood number for different parameters.

Pr	Ec	Nb	Nt	Df	Sc	Sr	Kr	$-\Theta(0)$	$-\varphi(0)$
5.0	0.2	0.3	0.8	1.2	0.8	0.5	0.3	0.54207	0.08890
7.0								0.53824	0.09971
9.0								0.53616	0.10554
6.2	0.1							0.50781	0.18830
	0.2							0.53946	0.09627
	0.3							0.57110	0.00424
	0.2	0.1						0.39941	0.16694
		0.2						0.46790	0.13298
		0.3						0.53945	0.09266
			1.0					0.51018	0.07099
			2.0					0.44849	0.06762
			3.0					0.42697	0.21223
			0.8	1.0				0.55726	0.04461
				1.5				0.52217	0.14643
				2.0				0.50539	0.19515
				1.2	0.3			0.45908	0.12628
					0.9			0.55407	0.09038
					1.5			0.63317	0.05616
					0.8	0.1		0.56699	0.08725
						0.5		0.53946	0.09627
						0.9		0.51777	0.10322
						0.5	0.1	0.47846	0.11703
							0.3	0.53946	0.09626
							0.5	0.60206	0.07332

6. Conclusions

This article examined the numerical solutions of two-dimensional, incompressible, electro-osmotic and Darcy-Forchheimer flow of the Maxwell nanofluid with the effects of electric and magnetic fields, Soret and Dufour effects, and chemical reaction over a porous medium. The results of these findings have been potentially used to improve industrial processes by increasing heat transfer in cooling systems, enhancing chemical reactor efficiency, refining filtering and separation procedures, expanding oil recovery technologies, and developing more effective medication delivery systems. Our research led us to the conclusions that:

- When the Maxwell fluid parameter, porosity parameter, Forchheimer number and electro-osmotic parameter are increased, the velocity profile decreases.
- The velocity develops as the magnetic parameter, electric field parameter and Helmholtz-Smoluchowski velocity rises.
- As the Prandtl number, thermophoresis parameter, and Dufour number rise, the temperature profile rises.
- The temperature profile narrows as the Eckert number rises.
- When the Brownian motion parameter, Schmidt number or chemical reaction parameter are increased, the concentration profile decreases.
- In the case where the Soret number grows, so does the concentration profile.
- The skin friction increases by 4% when the electric field parameter increases from 0.1 to 0.5. The Eckert number increases the Nusselt number by 35% and decreases the Sherwood number by 44%.

The future direction emphasizes the emergence of novel modelling approaches for industrial and technical applications, giving significant insights into the complicated behaviour of fluid flow which is investigated in this paper. Our work will focus on analysing how these effects impact the fluid flow behaviour and heat and mass transfer rates, and determining which parameters should be optimized to design more efficient systems, optimize processes, and improve material performance in fields such as nanotechnology, biotechnology and energy storage.

7. Limitation and future scope

When it comes to getting exact answers for boundary value problems, the fifth order Runge-Kutta method with the shooting technique is quite effective. However, in order to get the best convergence outcomes, one must be careful regarding initial guesses in the shooting technique. The applicability of this study's findings may be limited to specific conditions such as selected nanofluid, flow parameters and boundary conditions. Future research could expand upon this investigation by exploring various non-Newtonian fluids or hybrid models across various different geometries and certain analysis like sensitivity analysis, entropy generation and stability analysis can be performed.

References

[1] Choi, S.U.S., & Eastman, J.A. (1995). Enhancing thermal conductivity of fluids with nanoparticles. *ASME International Mechanical Engineering Congress & Exposition*, Nov. 12-17, San Francisco, USA.

[2] Wong, K.V. & De Leon, O. (2010). Applications of nanofluids: Current and future. *Advances in Mechanical Engineering*, 2, 519659. doi:10.1155/2010/519659

[3] Jama, M., Singh, T., Gamaledin, S.M., Koc, M., Samara, A., Isaifan, R.J., & Atieh, M.A. (2016). Crictical review on nanofluids: preparation, characterization, and applications. *Journal of Nanomaterials*, 2016(1), 717624. doi: 10.1155/2016/6717624

[4] De, P., Mondal, H., & Bera, U.K. (2016). Dual solutions of heat and mass transfer of nanofluid over a stretching/shrinking sheet with thermal radiation. *Meccanica*, 51,117−124. doi: 10.1007/s11012-015-0205-1

[5] Koriko, O.K., Shah, N.A., Saleem, S., Chung, J.D., Omowaye, A.J., & Oreyeni, T. (2021). Exploration of bioconvection flow of MHD thixotropic nanofluid past a vertical surface coexisting with both nanoparticles and gyrotactic microorganisms. *Scientific Reports*, 11, 16627. doi: 10.1038/s41598-021-96185-y

[6] Yaseen, M., Rawat, S.K., Shah, N.A., Kumar, M., & Eldin, S M. (2023). Ternary hybrid nanofluid flow containing gyrotactic microorganisms over three different geometries with Cattaneo-Christov model. *Mathematics*, 1(5), 1237. doi: 10.3390/math11051237

[7] Akram, M., Shahzad, M.H., Ahammad, N.A., Gamaoun, F., Awan, A.U., Hamam, H., & Alroobaea, R. (2024). Rheology of Eyring-Powell hybrid nanofluid flow under the peristaltic effects through an elliptical conduit: Analytical investigation. *Results in Physics*, 59, 107602. doi: 10.1016/j.rinp.2024.107602

[8] Shah, S.A.A., Qayyum, S., Nadeem, S., Alzubadi, H., Ahammad, N.A., Awan, A.U., & Alroobaea, R. (2025). Thermal characterization of Sutterby nanofluid flow under Riga plate: Tiwari and Das model. *Modern Physics Letters B*, 39(3) 2450421. doi: 10.1142/S0217984924504219

[9] Shahzad, M.H., Awan, A.U., Guedri, K., Fadhl, B.M., & Oreijah, M. (2024). Entropy-based investigation of blood flow in elliptical multi-stenotic artery with hybrid nanofluid in a fuzzy environment: Applications as drug carriers for brain diseases. *Engineering Applications of Artificial Intelligence*, 130, 107695. doi: 10.1016/j.engappai.2023.107695

[10] Akbar, A.A., Awan, A.U., Nadeem, S., Ahammad, N.A., Raza, N., Oreijah, M., Guedri, K. & Allahyani, S.A. (2024). Heat transfer analysis of Carreau-Yasuda nanofluid flow with variable thermal conductivity and quadratic convection. *Journal of Computational Design and Engineering*, 11(1), 99−109. doi: 10.1093/jcde/qwae009

[11] Hayat, T., Muhammad, T., Shehzad, S.A., Chen, G.Q., & Abbas, I.A. (2015). Interaction of magnetic field in flow of Maxwell nanofluid with convective effect. *Journal of Magnetism and Magnetic Materials*, 389, 48−55. doi: 10.1016/j.jmmm.2015.04.019.

[12] Nagendramma, V., Kumar, R.K., Prasad, P.D., Leelaratnam, A., & Varma, S.V. (2016). Multiple slips and radiation effects on Maxwell nanofluid flow over a permeable stretching surface with dissipation. *Journal of Nanofluids*, 5(6), 817−825. doi: 10.1166/jon.2016.1273.

[13] Jamshed, W. (2021). Numerical investigation of MHD impact on Maxwell nanofluid. *International Communications in Heat and Mass Transfer*, 120, 104973. doi: 10.1016/j.icheatmasstransfer.2020.104973

[14] Murtaza, S., Iftekhar, M., Ali, F., & Khan, I. (2020). Exact analysis of non-linear electro-osmotic flow of generalized Maxwell nanofluid: application in concrete based nano-materials. *IEEE Access*, 8, 96738-96747. doi: 10.1109/ACCESS.2020.2988259

[15] Sultana, N., Shaw, S., Nayak, M.K., & Mondal, S. (2023). Hydromagnetic slip flow and heat transfer treatment of Maxwell fluid with hybrid nanostructure: Low Prandtl numbers. *International Journal of Ambient Energy*, 44(1), 947−957. doi: 10.1080/01430750.2022.2158370

[16] Pantokratoras, A., & Magyari, E. (2009). EMHD free-convection boundary layer flow from a Riga-plate. *Journal of Engineering Mathematics*, 64, 303−315. doi: 10.1007/s10665-008-9259-6

[17] Buren, M. & Jian, Y. (2015). Electromagnetohydrodynamic (EMHD) flow between two transversely wavy microparallel plates. *Electrophoresis*, 36(14), 1539−1548. doi: 10.1002/elps.201500029

[18] Irfan, M., Farooq, M.A., & Iqra, T.A. (2020). A new computational technique design for EMHD nanofluid flow over a variable liquid characteristics. *Frontiers in Physics*, 8, 66. doi: 10.3389/fphy.2020.00066

[19] Muhammad Atif, S., Abbas, M., Rashid, U., & Emadifar, H. (2021). Stagnation point flow of EMHD micropolar nanofluid with mixed convection and slip boundary. *Complexity*, 2021(1), 3754922. doi: 10.1155/2021/3754922.

[20] Raptis, A. (1998). Radiation and free convection flow through a porous medium. *International Communications in Heat and Mass Transfer*, 25(2), 289−295. doi: 10.1016/S0735-1933(98)00016-5

[21] Hayat, T., Abbas, Z., Pop, I., & Asghar, S. (2010). Effects of radiation and magnetic field on the mixed convection stagnation-point flow over a vertical stretching sheet in a porous medium. *International Journal of Heat and Mass Transfer*, 53(1-3), 466−474. doi: 10.1016/j.ijheatmasstransfer.2009.09.010

[22] Qing, J., Bhatti, M.M., Abbas, M.A., Rashidi, M.M., & Ali, M.E. (2016). Entropy generation on MHD Casson nanofluid flow over a porous stretching/shrinking surface. *Entropy*, 18(4), 123. doi: 10.3390/ e18040123

[23] Sajid, T., Sagheer, M., Hussain, S., & Bilal, M. (2018). Darcy-Forchheimer flow of Maxwell nanofluid flow with nonlinear thermal radiation and activation energy. *AIP Advances*, 8(3), 035102. doi: 10.1063/1.5019218

[24] Sangeetha, E, & De, P. (2021). Darcy-Forchheimer porosity effects on nanofluid with motile gyrotactic microorganisms over convectively heated surface. *Nanoscience and Technology: An International Journal*, 12(4), 19−38. doi: 10.1615/NanoSciTechnolIntJ.2021037367

[25] Mohanty, D., Mahanta, G., Chamkha, A.J., & Shaw, S. (2023). Numerical analysis of interfacial nanolayer thickness on Darcy-Forchheimer Casson hybrid nanofluid flow over a moving needle with Cattaneo-Christov dual flux. *Numerical Heat Transfer, Part A: Applications*, 86(3), 399−423. doi: 10.1080/10407782.2023.2263906

[26] Mohanty, D., Sethy, N., Mahanta, G., & Shaw, S. (2023). Impact of the interfacial nanolayer on Marangoni convective Darcy-Forchheimer hybrid nanofluid flow over an infinite porous disk with Cattaneo-Christov heat flux. *Thermal Science and Engineering Progress, 41*, 101854. doi: 10.1016/j.tsep.2023.101854

[27] Mohanty, D., Mahanta, G., Byeon, H., Vignesh, S., Shaw, S., Khan, M. Ijaz, Abduvalieva, D., Govindan, V., Awwad, F.A., & Ismail, E.A.A. (2023). Thermo-solutal Marangoni convective Darcy-Forchheimer bio-hybrid nanofluid flow over a permeable disk with activation energy: Analysis of interfacial nanolayer thickness. *Open Physics*, 21(1), 20230119. doi: 10.1515/phys-2023-0119

[28] Sohail, M., El-Zahar, E.R., Mousa, A.A.A., Nazir, U., Althobaiti, S., Althobaiti, A., Shah, N.A., & Chung, J.D. (2022). Finite element analysis for ternary hybrid nanoparticles on thermal enhancement in pseudo-plastic liquid through porous stretching sheet. *Scientific Reports*, 12, 9219. doi: 10.1038/s41598-022-12857-3.

[29] Moorthy, M.B.K., & Senthilvadivu, K. (2012). Soret and Dufour effects on natural convection flow past a vertical surface in a porous medium with variable viscosity. *Journal of Applied Mathematics*, 2012(1), 634806. doi: 10.1155/2012/634806

[30] Partha, M.K., Murthy, P.V., & Raja Sehkhar, G.P. (2006). Soret and Dufour effects in a non-Darcy porous medium. *ASME Journal of Heat and Mass Transfer*, 128(6), 605−610. doi: 10.1115/1.2188512

[31] Ramzan, M., Bilal, M., Chung, J.D., & Farooq, U. (2016). Mixed convective flow of Maxwell nanofluid past a porous vertical stretched surface − An optimal solution. *Results in Physics*, 6, 1072−1079. doi: 10.1016/j.rinp.2016.11.036

[32] Venkateswarlu, B., & Narayana, P.V.S. (2017). Soret and Dufour effects on MHD flow of a Maxwell fluid over s stretching sheet with Joule heating. *Frontiers in Heat and Mass Transfer*, 9(11), 1−10. doi: 10.5098/hmt.9.11

[33] De, P. (2019). Soret-Dufour effects on unsteady flow of convective Eyring-Powell magneto nanofluids over a semi-infinite vertical plate. *BioNanoScience*, 9, 7−12. doi: 10.1007/s12668-018-0583-7

[34] Temjennaro, J., & Hemanta, K. (2023). Soret and Dufour effects on an unsteady MHD flow about a permeable rotating vertical cone with variable fluid properties. *Archives of Thermodynamics*, 45(1), 75−86. doi: 10.24425/ather.2024.150440

[35] Mathews, J., & Hymavathi, T. (2024). Unsteady magnetohydrodynamic free convection and heat transfer flow of Al2O3–Cu/water nanofluid over a non-linear stretching sheet in a porous medium. *Archives of Thermodynamics*, 45(1), 165–173. doi: 10.24425/ather.2024.150449

[36] Palaiah, S.S., Basha, H., Reddy, G.J, & Sheremet, M.A. (2021). Magnetized dissipative Soret effect on chemically reactive Maxwell fluid over a stretching sheet with joule heating. *Coatings*, 11(5), 528. doi: 10.3390/coatings11050528

[37] Zaher, A.Z., Ali, K.K., & Mekheimer, K.S. (2021). Electroosmosis forces EOF driven boundary layer flow for a non-Newtonian fluid with planktonic microorganism: Darcy Forchheimer model. *International Journal of Numerical Methods for Heat & Fluid Flow*, 31(8), 2534−2559. doi: 10.1108/HFF-10-2020-0666

[38] Abdelsalam, S.I., Mekheimer, K.S., & Zaher, A.Z. (2020). Alterations in blood stream by electroosmotic forces of hybrid nanofluid through diseased artery: Aneurysmal/stenosed segment. *Chinese Journal of Physics*, 67, 314−329. doi: 10.1016/j.cjph.2020.07.011

[39] Wang, C.Y. (1989). Free convection on a vertical stretching surface. *ZAMM - Journal of Applied Mathematics and Mechanics*, 69(11), 418−420. doi: 10.1007/BF00853952

[40] Reddy Gorla, R.S., & Sidawi, I. (1994). Free convection on a vertical stretching surface with suction and blowing. *Applied Scientific Research*, 52, 247-57. doi: 10.1007/BF00853952

[41] Khan, W.A., & Pop, I. (2010). Boundary-layer flow of a nanofluid past a stretching sheet. *International Journal of Heat and Mass Transfer*, 53(11−12), 2477−2483. doi: 10.1016/j.ijheatmasstransfer.2010.01.032.

[42] Hegazy, N., Eldabe, N.T., Abouzeid, M., Abousaleem, A., & Alana, A. (2023). Influence of both chemical reaction and electro-osmosis on MHD non-Newtonian fluid flow with gold nanoparticles. *Egyptian Journal of Chemistry*, 66(10), 191−201. doi: 10.21608/ejchem.2023.190175.7526

[43] Kumar, K.G., Gireesha, B.J., Rudraswamy, N.G., & Krishnamurthy, M.R. (2019). An unsteady flow and melting heat transfer of a nanofluid over a stretching sheet embedded in a porous medium. *International Journal of Applied Mechanics and Engineering*, 24(2), 245−258. doi: 10.2478/ijame-2019-0016

[44] Palanimani, P.G. (2007). Effects of chemical reactions, heat, and mass transfer on nonlinear magnetohydrodynamic boundary layer flow over a wedge with a porous medium in the presence of ohmic heating and viscous dissipation. *Journal of Porous Media*, 10(5), 489−502. doi: 10.1615/JPorMedia.v10.i5.60

[45] Ragupathi, P., Ahammad, N.A., Wakif, A., Shah, N.A., & Jeon, Y. (2022). Exploration of multiple transfer phenomena within viscous fluid flows over a curved stretching sheet in the co-existence of gyrotactic micro-organisms and tiny particles. *Mathematics*, 10(21), 4133. doi: 10.3390/math10214133

[46] Awan, A.U., Qayyum, S., Nadeem, S., Ahammad, N.A., Gepreel, K.A., Alharthi, M., & Alosaimi, M. (2024). Analysis of chemical characteristics of engine-oil-based Prandtl hybrid nanofluid flow. *ZAMM - Journal of Applied Mathematics and Mechanics/Zeitschrift für Angewandte Mathematik und Mechanik*, 104(8), e202400050. doi: 10.1002/zamm.202400050

[47] Raza, Q., Qureshi, M.Z.A., Khan, B.A., Kadhim Hussein, A., Ali, B., Shah, N.A., & Chung, J.D. (2022). Insight into dynamic of mono and hybrid nanofluids subject to binary chemical reaction, activation energy, and magnetic field through the porous surfaces. *Mathematics*, 10(16), 3013. doi: 10.3390/math10163013